Power Minimization of Multiuser FAS-RIS Downlink System

Boyi Tang, *Student Member, IEEE*, Hao Xu, *Senior Member, IEEE*, Kai-Kit Wong, *Fellow, IEEE*, Li You, *Senior Member, IEEE*, Jie Tang, *Senior Member, IEEE*, Yangyang Zhang, and Hyundong Shin, *Fellow, IEEE*

***Abstract*—Both fluid antenna system (FAS) and reconfigurable intelligent surface (RIS) are promising technologies that enhance the performance of wireless communications. This letter studies the power minimization problem under quality of service (QoS) constraints in a multiuser FAS-RIS-aided system, where each user is equipped with a planar FAS, and the base station (BS) has multiple fixed-position antennas (FPAs). The precoding vectors, the RIS elements, and the user antenna positions are iteratively optimized to minimize the transmit power. Our simulation results show that the proposed approaches require much less transmit power to achieve the QoS than the FPA counterpart.**

***Index Terms*—Fluid antenna system, reconfigurable intelligent surface, antenna position optimization, power minimization.**

I. Introduction

FLUID antenna system (FAS) has recently been proposed to greatly improve spatial diversity and enable massive connectivity, e.g., [1], [2], [3]. FAS represents any form of shape-flexible, position-flexible antenna systems [4], [5], such as liquid-based antenna [6], RF pixel-based antenna [7], metamaterial based antenna [8], and movable antenna [9]. FAS has also innovated multiple access by enabling users to access the highs and lows of the fading envelopes in the spatial domain. The concept of fluid antenna multiple access (FAMA) can be interpreted as 'beamforming by nature' to mitigate inter-user interference, without actually performing beamforming at the transmitter [4]. In [10], the outage probability for two-user FAMA was analyzed while [11] tackled the energy efficiency problem of a multiuser FAMA through a mean-field game.

Recent efforts also combined FAS with other technologies. Fairness issues of non-orthogonal multiple access and orthogonal multiple access systems using FAS were recently addressed in [12]. In [13], [14], the authors studied the performance of FAS in improving the integrated sensing and communication (ISAC) systems. The system delay of mobile edge computing networks was investigated in [15]. Reinforcement learning was employed in [16] to maximize the sum rate for opportunistic FAMA systems. FAS was further considered as a relay in [17], showing improvement in the sum rate by 125%. In [18], FAS-aided wireless information and power transfer was evaluated under imperfect channel state information (CSI).

The work of K. K. Wong is supported by the Engineering and Physical Sciences Research Council (EPSRC) under grant EP/W026813/1.

B. Tang and K. Wong are with the Department of Electronic and Electrical Engineering, University College London, London WC1E7JE, U.K., (e-mail: {boyi.tang.22, kai-kit.wong}@ucl.ac.uk). K. Wong is also affiliated with the Department of Electronic Engineering, Kyung Hee University, Yongin-si, Gyeonggi-do 17104, South Korea.

H. Xu and L. You are with the National Mobile Communications Research Laboratory, Southeast University, Nanjing 210096, China, (e-mail: {hao.xu, lyou}@seu.edu.cn). L. You is also with the Purple Mountain Laboratories, Nanjing 211100, China.

J. Tang is with the School of Electronic and Information Engineering, South China University of Technology, Guangzhou 510641, China, (e-mail: eejtang@scut.edu.cn).

Y. Zhang is with Kuang-Chi Science Limited, Hong Kong SAR, China, (e-mail: yangyang.zhang@kuang-chi.org).

H. Shin is affiliated with the Department of Electronics and Information Convergence Engineering, Kyung Hee University, Yongin-si, Gyeonggi-do 17104, South Korea (e-mail: hshin@khu.ac.kr).

Corresponding authors: Hao Xu and Kai-Kit Wong.

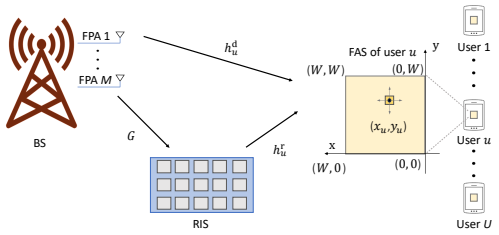

Fig. 1. A multiuser FAS-RIS-aided system where the users and the BS are equipped with 2D fluid antennas and FPAs, respectively.

On the other hand, reconfigurable intelligent surface (RIS) is a promising technology that improves wireless communication coverage with low power consumption, e.g., [19], [20]. However, the cascaded channel fading effect in RIS systems often leads to a reduction in received signal power, posing a significant challenge. In this context, FAS can provide users more spatial degrees of freedom (DoF) to effectively reduce the effect of noise. The performance analysis of RIS-aided FAS was first given in [21]. The sum-rate maximization problems of RIS-assisted systems were investigated in [22] and [23], where the FASs were equipped on the unmanned aerial vehicle (UAV) and the base station (BS), respectively. The authors of [24] investigated FAS and RIS-assisted index modulation in a millimeter-wave system, and proposed a transmission scheme with low hardware cost and power consumption to improve the error performance and the spectral efficiency. The impact of equipping position-flexible elements on RIS was evaluated in [25], [26]. However, the power minimization problem of a FAS-RIS-assisted multiuser system has not been studied.

This letter studies the transmit power minimization problem of a FAS-RIS-aided downlink system in which the users and the BS are equipped with a single-antenna FAS and multiple fixed-position antennas (FPAs), respectively. Due to non-convexity, we iteratively optimize the precoding vectors, phase shift of the RIS, and the user antenna positions. Simulation results show that FAS can achieve the quality of service (QoS) constraints with much less power than FPA.

II. System Model

A. Signal Model

We consider a FAS-RIS-assisted downlink system as shown in Fig. 1, where the BS transmits messages to U users on the same physical channel. Each user is equipped with a single-antenna two-dimensional (2D) FAS of size $\mathcal{S} = [0, W] \times [0, W]$ while the BS has M FPAs. In the FAS, the antenna can be instantly switched to any position within the given region. We also consider a RIS with a passive reflecting uniform planar array (UPA) of dimension $N = N_1 \times N_2$ in the system to assist the communication from the BS to the users.

Let $\boldsymbol{w}_u \in \mathbb{C}^{M\times 1}$ and $\boldsymbol{v}_u = [x_u, y_u]^T$ represent the precoding vector and the antenna position of user u, respectively. Then the received signal at the u-th user is given by

$$z_u = (\boldsymbol{h}_u^{\mathrm{r}}(\boldsymbol{v}_u)\boldsymbol{\Theta}\boldsymbol{G} + \boldsymbol{h}_u^{\mathrm{d}}(\boldsymbol{v}_u))\sum_{k=1}^{U}\boldsymbol{w}_k s_k + n_u, \tag{1}$$

where $s_u \sim \mathcal{CN}(0,1)$ is the symbol for user u, $\boldsymbol{h}_u^{\mathrm{d}}(\boldsymbol{v}_u) \in \mathbb{C}^{1\times M}$ and $\boldsymbol{h}_u^{\mathrm{r}}(\boldsymbol{v}_u) \in \mathbb{C}^{1\times N}$ are respectively the direct channel from the BS to user u and the RIS-user u channel, the diagonal matrix $\boldsymbol{\Theta} = \mathrm{diag}(e^{j\theta_1}, \ldots, e^{j\theta_N})$ is the reflection-coefficients matrix of the RIS, $\boldsymbol{G} \in \mathbb{C}^{N\times M}$ is the channel between the BS and the RIS, and $n_u \sim \mathcal{CN}(0, \sigma_u^2)$ is the additive noise. Denote the user index set by $\mathcal{U} = \{1, \ldots, U\}$. The signal-to-interference-plus-noise ratio (SINR) at user u is given by

$$\eta_u(\boldsymbol{w}_{\mathcal{U}}, \boldsymbol{\Theta}, \boldsymbol{v}_u) = \frac{\left|(\boldsymbol{h}_u^{\mathrm{r}}(\boldsymbol{v}_u)\boldsymbol{\Theta}\boldsymbol{G} + \boldsymbol{h}_u^{\mathrm{d}}(\boldsymbol{v}_u))\boldsymbol{w}_u\right|^2}{\sum_{k\neq u}\left|(\boldsymbol{h}_u^{\mathrm{r}}(\boldsymbol{v}_u)\boldsymbol{\Theta}\boldsymbol{G} + \boldsymbol{h}_u^{\mathrm{d}}(\boldsymbol{v}_u))\boldsymbol{w}_k\right|^2 + \sigma_u^2}. \tag{2}$$

B. Channel Model

1) BS-user channel: Denote the number of propagation paths of the BS-user u direct channel by L_u^{d}, and the complex channel gain of the l-th path by $\gamma_{u,l}^{\mathrm{d}} \sim \mathcal{CN}(0,1)$. Using the geometric channel model, the direct channel between the BS and user u can be modeled as [27]

$$\boldsymbol{h}_u^{\mathrm{d}}(\boldsymbol{v}_u) = \sum_{l=1}^{L_u^{\mathrm{d}}}\gamma_{u,l}^{\mathrm{d}} r_{u,l}^{\mathrm{d}}(\boldsymbol{v}_u)\left(\boldsymbol{t}_{u,l}^{\mathrm{d}}\right)^H, \tag{3}$$

where $\boldsymbol{t}_{u,l}^{\mathrm{d}}$ and $r_{u,l}^{\mathrm{d}}$ denote the steering vector at the BS side and the steering element at the user side, respectively, and the superscript 'd' indicates that it is the direct link between the BS and the user. Denote the angle of departure (AoD) of the l-th path from the BS to user u by $\zeta_{u,l}^{\mathrm{d}}$. Then we have

$$\boldsymbol{t}_{u,l}^{\mathrm{d}} = \left[1, e^{-j\frac{2\pi}{\lambda}d_{\mathrm{BS}}\cos\zeta_{u,l}^{\mathrm{d}}}, \ldots, e^{-j\frac{2\pi}{\lambda}(M-1)d_{\mathrm{BS}}\cos\zeta_{u,l}^{\mathrm{d}}}\right]^T, \tag{4}$$

where λ is the wavelength and d_{BS} is the BS antenna spacing.

For the BS-user u channel, the azimuth and elevation angles of arrival (AoAs) of the l-th path are denoted by $\phi_{u,l}^{\mathrm{d}}$ and $\theta_{u,l}^{\mathrm{d}}$, respectively. The distance difference in the l-th path of the BS-user u channel between $\boldsymbol{v}_u$ and its origin $[0,0]^T$ is

$$\rho_{u,l}^{\mathrm{d}}(\boldsymbol{v}_u) = x_u \sin\theta_{u,l}^{\mathrm{d}}\cos\phi_{u,l}^{\mathrm{d}} + y_u\cos\theta_{u,l}^{\mathrm{d}}. \tag{5}$$

As a consequence, the steering element at user u is $r_{u,l}^{\mathrm{d}}(\boldsymbol{v}_u) = e^{-j\frac{2\pi}{\lambda}\rho_{u,l}^{\mathrm{d}}(\boldsymbol{v}_u)}$. Now, we denote

$$\begin{cases}\boldsymbol{r}_u^{\mathrm{d}}(\boldsymbol{v}_u) = \left[r_{u,1}^{\mathrm{d}}(\boldsymbol{v}_u), \ldots, r_{u,L_u^{\mathrm{d}}}^{\mathrm{d}}(\boldsymbol{v}_u)\right] \in \mathbb{C}^{1\times L_u^{\mathrm{d}}},\\ \boldsymbol{\Gamma}_u^{\mathrm{d}} = \mathrm{diag}\{\gamma_{u,1}^{\mathrm{d}}, \ldots, \gamma_{u,L_u^{\mathrm{d}}}^{\mathrm{d}}\} \in \mathbb{C}^{L_u^{\mathrm{d}}\times L_u^{\mathrm{d}}},\\ \boldsymbol{T}_u^{\mathrm{d}} = \left[\boldsymbol{t}_{u,1}^{\mathrm{d}}(\boldsymbol{w}_u), \ldots, \boldsymbol{t}_{u,L_u^{\mathrm{d}}}^{\mathrm{d}}(\boldsymbol{w}_u)\right] \in \mathbb{C}^{M\times L_u^{\mathrm{d}}},\end{cases} \tag{6}$$

based on which (3) can be rewritten in matrix form as

$$\boldsymbol{h}_u^{\mathrm{d}}(\boldsymbol{v}_u) = \boldsymbol{r}_u^{\mathrm{d}}(\boldsymbol{v}_u)\boldsymbol{\Gamma}_u^{\mathrm{d}}\left(\boldsymbol{T}_u^{\mathrm{d}}\right)^H. \tag{7}$$

2) BS-RIS channel: Denote the number of paths, AoD, and azimuth-elevation AoAs of the BS-RIS channel by L_{br}, ζ_l^{br}, and $(\phi_l^{\mathrm{br}}, \theta_l^{\mathrm{br}})$, respectively, where the superscript 'br' indicates that it is the link between the BS and RIS. Denote $\varpi_l^{\mathrm{br}} = \sin\theta_l^{\mathrm{br}}\cos\phi_l^{\mathrm{br}}$. The steering vectors of the BS and the RIS are, respectively, written as

$$\begin{cases}\boldsymbol{t}_l^{\mathrm{br}} = \left[1, e^{-j\frac{2\pi}{\lambda}d_{\mathrm{BS}}\cos\zeta_l^{\mathrm{br}}}, \ldots, e^{-j\frac{2\pi}{\lambda}(M-1)d_{\mathrm{BS}}\cos\zeta_l^{\mathrm{br}}}\right]^T,\\ \boldsymbol{r}_l^{\mathrm{br}} = \boldsymbol{r}_l^{\mathrm{br}_1}\otimes\boldsymbol{r}_l^{\mathrm{br}_2},\end{cases} \tag{8}$$

where

$$\begin{cases}\boldsymbol{r}_l^{\mathrm{br}_1} = \left[1, e^{-j\frac{2\pi}{\lambda}d_{\mathrm{r}}\cos\theta_l^{\mathrm{br}}}, \ldots, e^{-j\frac{2\pi}{\lambda}(N_1-1)d_{\mathrm{r}}\cos\theta_l^{\mathrm{br}}}\right]^T,\\ \boldsymbol{r}_l^{\mathrm{br}_2} = \left[1, e^{-j\frac{2\pi}{\lambda}d_{\mathrm{r}}\varpi_l^{\mathrm{br}}}, \ldots, e^{-j\frac{2\pi}{\lambda}(N_2-1)d_{\mathrm{r}}\varpi_l^{\mathrm{br}}}\right]^T,\end{cases} \tag{9}$$

are respectively the steering vectors with respect to the vertical direction and horizontal direction of the RIS, d_{r} is the RIS element spacing. Let $\gamma_l^{\mathrm{br}} \sim \mathcal{CN}(0,1)$ denote the complex channel gain. Then the BS-RIS channel can be written as

$$\boldsymbol{G} = \boldsymbol{R}_{\mathrm{br}}\boldsymbol{\Gamma}_{\mathrm{br}}\boldsymbol{T}_{\mathrm{br}}^H, \tag{10}$$

where

$$\begin{cases}\boldsymbol{R}_{\mathrm{br}} = \left[\boldsymbol{r}_1^{\mathrm{br}}, \ldots, \boldsymbol{r}_{L_{\mathrm{br}}}^{\mathrm{br}}\right] \in \mathbb{C}^{N\times L_{\mathrm{br}}},\\ \boldsymbol{\Gamma}_{\mathrm{br}} = \mathrm{diag}\{\gamma_1^{\mathrm{br}}, \ldots, \gamma_{L_{\mathrm{br}}}^{\mathrm{br}}\} \in \mathbb{C}^{L_{\mathrm{br}}\times L_{\mathrm{br}}},\\ \boldsymbol{T}_{\mathrm{br}} = \left[\boldsymbol{t}_1^{\mathrm{br}}, \ldots, \boldsymbol{t}_{L_{\mathrm{br}}}^{\mathrm{br}}\right] \in \mathbb{C}^{M\times L_{\mathrm{br}}}.\end{cases} \tag{11}$$

3) RIS-user channel: Similarly, for the RIS-user u channel, the number of propagation paths, and the azimuth and elevation AoDs of the l-th path from the RIS to user u are denoted by L_u^{r}, $\xi_{u,l}^{\mathrm{r}}$, and $\zeta_{u,l}^{\mathrm{r}}$, respectively, where the superscript 'r' indicates that it is the link between RIS and the user. Denote $\varpi_{u,l}^{\mathrm{r}} = \sin\zeta_{u,l}^{\mathrm{r}}\cos\xi_{u,l}^{\mathrm{r}}$. The steering vector of the RIS-user u channel is given by

$$\boldsymbol{t}_{u,l}^{\mathrm{r}} = \boldsymbol{t}_{u,l}^{\mathrm{r}_1}\otimes\boldsymbol{t}_{u,l}^{\mathrm{r}_2}, \tag{12}$$

where

$$\begin{cases}\boldsymbol{t}_{u,l}^{\mathrm{r}_1} = \left[1, e^{-j\frac{2\pi}{\lambda}d_{\mathrm{r}}\cos\zeta_{u,l}^{\mathrm{r}}}, \ldots, e^{-j\frac{2\pi}{\lambda}(N_1-1)d_{\mathrm{r}}\cos\zeta_{u,l}^{\mathrm{r}}}\right]^T,\\ \boldsymbol{t}_{u,l}^{\mathrm{r}_2} = \left[1, e^{-j\frac{2\pi}{\lambda}d_{\mathrm{r}}\varpi_{u,l}^{\mathrm{r}}}, \ldots, e^{-j\frac{2\pi}{\lambda}(N_2-1)d_{\mathrm{r}}\varpi_{u,l}^{\mathrm{r}}}\right]^T.\end{cases} \tag{13}$$

Denote the azimuth-elevation AoAs of the l-th path by $(\phi_{u,l}^{\mathrm{r}}, \theta_{u,l}^{\mathrm{r}})$. The steering element of the RIS-user channel at user u is $r_{u,l}^{\mathrm{r}}(\boldsymbol{v}_u) = e^{-j\frac{2\pi}{\lambda}\rho_{u,l}^{\mathrm{r}}(\boldsymbol{v}_u)}$, where

$$\rho_{u,l}^{\mathrm{r}}(\boldsymbol{v}_u) = x_u\sin\theta_{u,l}^{\mathrm{r}}\cos\phi_{u,l}^{\mathrm{r}} + y_u\cos\theta_{u,l}^{\mathrm{r}}. \tag{14}$$

Then the RIS-user u channel can be modeled as

$$\boldsymbol{h}_u^{\mathrm{r}}(\boldsymbol{v}_u) = \sum_{l=1}^{L_u^{\mathrm{r}}}\gamma_{u,l}^{\mathrm{r}} r_{u,l}^{\mathrm{r}}(\boldsymbol{v}_u)\left(\boldsymbol{t}_{u,l}^{\mathrm{r}}\right)^H, \tag{15}$$

where $\gamma_{u,l}^{\mathrm{r}} \sim \mathcal{CN}(0,1)$ is the complex channel gain. Similar to the BS-user channel, (15) can be rewritten as

$$\boldsymbol{h}_u^{\mathrm{r}}(\boldsymbol{v}_u) = \boldsymbol{r}_u^{\mathrm{r}}(\boldsymbol{v}_u)\boldsymbol{\Gamma}_u^{\mathrm{r}}\left(\boldsymbol{T}_u^{\mathrm{r}}\right)^H, \tag{16}$$

where

$$\begin{cases} \boldsymbol{r}_u^{\mathrm{r}}(\boldsymbol{v}_u) = \left[r_{u,1}^{\mathrm{r}}(\boldsymbol{v}_u), \ldots, r_{u,L_u^{\mathrm{r}}}^{\mathrm{r}}(\boldsymbol{v}_u)\right] \in \mathbb{C}^{1\times L_u^{\mathrm{r}}}, \\ \boldsymbol{\Gamma}_u^{\mathrm{r}} = \mathrm{diag}\{\gamma_{u,1}^{\mathrm{r}}, \ldots, \gamma_{u,L_u^{\mathrm{r}}}^{\mathrm{r}}\} \in \mathbb{C}^{L_u^{\mathrm{r}}\times L_u^{\mathrm{r}}}, \\ \boldsymbol{T}_u^{\mathrm{r}} = \left[\boldsymbol{t}_{u,1}^{\mathrm{r}}(\boldsymbol{w}_u), \ldots, \boldsymbol{t}_{u,L_u^{\mathrm{r}}}^{\mathrm{r}}(\boldsymbol{w}_u)\right] \in \mathbb{C}^{N\times L_u^{\mathrm{r}}}. \end{cases} \tag{17}$$

C. Problem Formulation

Our aim is to minimize the transmit power by optimizing the precoding vectors $\boldsymbol{w}_{\mathcal{U}}$, the phase shift matrix of the RIS $\boldsymbol{\Theta}$, and the antenna positions $\boldsymbol{v}_{\mathcal{U}}$ of all the users. Mathematically, the problem can be formulated as

$$\min_{\boldsymbol{w}_{\mathcal{U}},\boldsymbol{\Theta},\boldsymbol{v}_{\mathcal{U}}} \sum_{u=1}^{U} \|\boldsymbol{w}_u\|^2 \ \text{ s.t. } \begin{cases} \eta_u(\boldsymbol{w}_{\mathcal{U}},\boldsymbol{\Theta},\boldsymbol{v}_u) \geq \epsilon_u, \forall u \in \mathcal{U}, \\ \boldsymbol{v}_u \in \mathcal{S}, \ \forall u \in \mathcal{U}, \\ 0 \leq \theta_n \leq 2\pi, \ \forall n \in \mathcal{N}, \end{cases} \tag{18}$$

where ϵ_u is the SINR target for user u and $\mathcal{N} = \{1, \ldots, N\}$.

III. Proposed Solution

A. Alternative Optimization

Since (18) is non-convex, we alternatively optimize $\boldsymbol{w}_{\mathcal{U}}$, $\boldsymbol{\Theta}$, and $\boldsymbol{v}_{\mathcal{U}}$. For given $\boldsymbol{v}_{\mathcal{U}}$, (18) is a classical optimization problem for RIS. Thus, we optimize $\boldsymbol{w}_{\mathcal{U}}$ and $\boldsymbol{\Theta}$ using the approach in [19]. For given $\boldsymbol{w}_{\mathcal{U}}$ and $\boldsymbol{\Theta}$, (18) becomes

$$\min_{\boldsymbol{v}_{\mathcal{U}}} \sum_{u=1}^{U} \|\boldsymbol{w}_u\|^2 \ \text{ s.t. } \begin{cases} \eta_u(\boldsymbol{v}_u) \geq \epsilon_u, \ \forall u \in \mathcal{U}, \\ \boldsymbol{v}_u \in \mathcal{S}, \ \forall u \in \mathcal{U}. \end{cases} \tag{19}$$

For convenience, we denote $\boldsymbol{h}_u^{\mathrm{r}}(\boldsymbol{v}_u)\boldsymbol{\Theta}\boldsymbol{G}+\boldsymbol{h}_u^{\mathrm{d}}(\boldsymbol{v}_u)$ by $\boldsymbol{h}_u(\boldsymbol{v}_u)$. Then, based on (2), the SINR constraint can be equivalently rewritten as

$$|\boldsymbol{h}_u(\boldsymbol{v}_u)\boldsymbol{w}_u|^2 - \epsilon_u\left(\sum_{k\neq u}^{U} |\boldsymbol{h}_u(\boldsymbol{v}_u)\boldsymbol{w}_k|^2 + \sigma_u^2\right) \geq 0, \forall u \in \mathcal{U}. \tag{20}$$

As the SINR constraint is still non-convex, we move it into the objective function by introducing a penalty τ and get

$$\min_{\boldsymbol{v}_{\mathcal{U}}} \sum_{u=1}^{U} \|\boldsymbol{w}_u\|^2 - \tau \sum_{u=1}^{U} \left[|\boldsymbol{h}_u(\boldsymbol{v}_u)\boldsymbol{w}_u|^2 - \epsilon_u \sum_{k\neq u}^{U} |\boldsymbol{h}_u(\boldsymbol{v}_u)\boldsymbol{w}_k|^2 - \epsilon_u\sigma_u^2\right]$$
$$\text{s.t. } \ \boldsymbol{v}_u \in \mathcal{S}, \ \forall u \in \mathcal{U}. \tag{21}$$

Dropping the constants, (21) can be transformed to

$$\max_{\boldsymbol{v}_{\mathcal{U}}} \sum_{u=1}^{U} \left[|\boldsymbol{h}_u(\boldsymbol{v}_u)\boldsymbol{w}_u|^2 - \epsilon_u \sum_{k\neq u}^{U} |\boldsymbol{h}_u(\boldsymbol{v}_u)\boldsymbol{w}_k|^2\right]$$
$$\text{s.t. } \ \boldsymbol{v}_u \in \mathcal{S}, \ \forall u \in \mathcal{U}. \tag{22}$$

As the antenna position of each user is independent, (22) can be decomposed into U subproblems. For user u, we have the corresponding objective function

$$\begin{aligned} f(\boldsymbol{v}_u) &\triangleq \boldsymbol{h}_u(\boldsymbol{v}_u)\boldsymbol{w}_u\boldsymbol{w}_u^H\boldsymbol{h}_u^H(\boldsymbol{v}_u) - \epsilon_u \sum_{k\neq u}^{U} \boldsymbol{h}_u(\boldsymbol{v}_u)\boldsymbol{w}_k\boldsymbol{w}_k^H\boldsymbol{h}_u^H(\boldsymbol{v}_u) \\ &= (\boldsymbol{h}_u^{\mathrm{r}}(\boldsymbol{v}_u)\boldsymbol{\Theta}\boldsymbol{G} + \boldsymbol{h}_u^{\mathrm{d}}(\boldsymbol{v}_u))\boldsymbol{W}_u(\boldsymbol{h}_u^{\mathrm{r}}(\boldsymbol{v}_u)\boldsymbol{\Theta}\boldsymbol{G} + \boldsymbol{h}_u^{\mathrm{d}}(\boldsymbol{v}_u))^H \\ &= \boldsymbol{r}_u^{\mathrm{r}}(\boldsymbol{v}_u)\boldsymbol{A}_u\boldsymbol{r}_u^{\mathrm{r}}(\boldsymbol{v}_u)^H + \boldsymbol{r}_u^{\mathrm{r}}(\boldsymbol{v}_u)\boldsymbol{B}_u\boldsymbol{r}_u^{\mathrm{d}}(\boldsymbol{v}_u)^H \\ &\quad + \boldsymbol{r}_u^{\mathrm{d}}(\boldsymbol{v}_u)\boldsymbol{C}_u\boldsymbol{r}_u^{\mathrm{r}}(\boldsymbol{v}_u)^H + \boldsymbol{r}_u^{\mathrm{d}}(\boldsymbol{v}_u)\boldsymbol{D}_u\boldsymbol{r}_u^{\mathrm{d}}(\boldsymbol{v}_u)^H, \end{aligned} \tag{23}$$

in which we have $\boldsymbol{W}_u = \boldsymbol{w}_u\boldsymbol{w}_u^H - \epsilon_u\sum_{k\neq u}^{U}\boldsymbol{w}_k\boldsymbol{w}_k^H$, $\boldsymbol{A}_u = \boldsymbol{\Gamma}_u^{\mathrm{r}}\boldsymbol{T}_u^{\mathrm{r}H}\boldsymbol{\Theta}\boldsymbol{G}\boldsymbol{W}_u\boldsymbol{G}^H\boldsymbol{\Theta}^H\boldsymbol{T}_u^{\mathrm{r}}\boldsymbol{\Gamma}_u^{\mathrm{r}H}$, $\boldsymbol{B}_u = \boldsymbol{\Gamma}_u^{\mathrm{r}}\boldsymbol{T}_u^{\mathrm{r}H}\boldsymbol{\Theta}\boldsymbol{G}\boldsymbol{W}_u\boldsymbol{T}_u^{\mathrm{d}}\boldsymbol{\Gamma}_u^{\mathrm{d}H}$, $\boldsymbol{C}_u = \boldsymbol{\Gamma}_u^{\mathrm{d}}\boldsymbol{T}_u^{\mathrm{d}H}\boldsymbol{W}_u\boldsymbol{G}^H\boldsymbol{\Theta}^H\boldsymbol{T}_u^{\mathrm{r}}\boldsymbol{\Gamma}_u^{\mathrm{r}H}$, and $\boldsymbol{D}_u = \boldsymbol{\Gamma}_u^{\mathrm{d}}\boldsymbol{T}_u^{\mathrm{d}H}\boldsymbol{W}_u\boldsymbol{T}_u^{\mathrm{d}}\boldsymbol{\Gamma}_u^{\mathrm{d}H}$. Therefore, we rewrite (22) as U subproblems, where the u-th subproblem is written as

$$\max_{\boldsymbol{v}_u} f(\boldsymbol{v}_u) \ \text{ s.t. } \ \boldsymbol{v}_u \in \mathcal{S}. \tag{24}$$

If $\forall u \in \mathcal{U}$, the solution of (24) satisfies $\eta_u(\boldsymbol{v}_u) \geq \epsilon_u$, (19) is solved. Otherwise, (19) is infeasible. In the following, we propose three methods to solve (24).

1) Discrete Exhaustive Search (ES): As $\boldsymbol{v}_u \in \mathcal{S}$, a near-optimal solution can be obtained by discrete ES [28], [29]. In particular, we divide the entire space of FAS equally into K^2 small squares with $(K+1)^2$ vertices. The coordinates of the vertices are contained in the potential position set of the FAS $\mathcal{X} = \{0, d_{\mathrm{FAS}}, 2d_{\mathrm{FAS}}, \ldots, W\} \times \{0, d_{\mathrm{FAS}}, 2d_{\mathrm{FAS}}, \ldots, W\}$, where $d_{\mathrm{FAS}} = W/K$ is the search step. Then, for each user u, we take the point in $\mathcal{X}$ that yields the maximum $f(\boldsymbol{v}_u)$ as the solution of problem (24), i.e.,

$$\boldsymbol{v}_u^* = \arg\max_{\hat{\boldsymbol{v}}_u \in \mathcal{X}} f(\hat{\boldsymbol{v}}_u). \tag{25}$$

Since the computational complexity of ES is high for large K, we propose the following two methods.

2) Successive Convex Approximation (SCA) based Method: As (24) is non-convex and intractable, we successively approximate it in a convex form [30]. According to the second-order Taylor expansion, we can obtain a lower-bound of $f(\boldsymbol{v}_u)$ as

$$\begin{aligned} f(\boldsymbol{v}_u) &\geq f(\boldsymbol{v}_u^{(i)}) + \nabla f(\boldsymbol{v}_u^{(i)})^T(\boldsymbol{v}_u - \boldsymbol{v}_u^{(i)}) - \frac{\delta_u}{2}(\boldsymbol{v}_u - \boldsymbol{v}_u^{(i)})^T(\boldsymbol{v}_u - \boldsymbol{v}_u^{(i)}) \\ &= -\frac{\delta_u}{2}\boldsymbol{v}_u^T\boldsymbol{v}_u + \left(\delta_u\boldsymbol{v}_u^{(i)} + \nabla f(\boldsymbol{v}_u^{(i)})\right)^T\boldsymbol{v}_u \\ &\quad - \frac{\delta_u}{2}(\boldsymbol{v}_u^{(i)})^T\boldsymbol{v}_u^{(i)} - \nabla f(\boldsymbol{v}_u^{(i)})^T\boldsymbol{v}_u^{(i)} + f(\boldsymbol{v}_u^{(i)}), \end{aligned} \tag{26}$$

where $\boldsymbol{v}_u^{(i)}$ is the value of $\boldsymbol{v}_u$ obtained in the i-th iteration and δ_u is a positive real number satisfying $\delta_u\boldsymbol{I}_2 \succeq \nabla^2 f(\boldsymbol{v}_u)$.

To employ the Taylor series expansion above, we provide the gradient of $f(\boldsymbol{v}_u)$ and the value of δ_u as follows. Denoting the (i,l)-th element of $\boldsymbol{A}_u, \boldsymbol{B}_u, \boldsymbol{C}_u, \boldsymbol{D}_u$ in (23) by $a_u^{i,l}, b_u^{i,l}, c_u^{i,l}, d_u^{i,l}$, respectively, we have

$$\begin{aligned} f(\boldsymbol{v}_u) &= \sum_{i=1}^{L_u^{\mathrm{r}}}\sum_{l=1}^{L_u^{\mathrm{r}}} a_u^{i,l}\psi(u,\mathrm{r},l,\mathrm{r},i) + \sum_{i=1}^{L_u^{\mathrm{r}}}\sum_{l=1}^{L_u^{\mathrm{d}}} b_u^{i,l}\psi(u,\mathrm{d},l,\mathrm{r},i) \\ &+ \sum_{i=1}^{L_u^{\mathrm{d}}}\sum_{l=1}^{L_u^{\mathrm{r}}} c_u^{i,l}\psi(u,\mathrm{r},l,\mathrm{d},i) + \sum_{i=1}^{L_u^{\mathrm{d}}}\sum_{l=1}^{L_u^{\mathrm{d}}} d_u^{i,l}\psi(u,\mathrm{d},l,\mathrm{d},i), \end{aligned} \tag{27}$$

where $\psi(u,\chi_1,l,\chi_2,i) = e^{j\frac{2\pi}{\lambda}\left(\rho_{u,l}^{\chi_1}(\boldsymbol{v}_u) - \rho_{u,i}^{\chi_2}(\boldsymbol{v}_u)\right)}$ and $\chi_1, \chi_2 \in \{\mathrm{d}, \mathrm{r}\}$. Denote $g_1(\theta_1,\phi_1,\theta_2,\phi_2) = \sin\theta_1\cos\phi_1 - \sin\theta_2\cos\phi_2$, $g_2(\theta_1,\theta_2) = \cos\theta_1 - \cos\theta_2$. The gradient of $f(\boldsymbol{v}_u)$ over $\boldsymbol{v}_u$ can be found as

$$\nabla f(\boldsymbol{v}_u) = \left[\frac{\partial f(\boldsymbol{v}_u)}{\partial x_u}, \frac{\partial f(\boldsymbol{v}_u)}{\partial y_u}\right]^T, \tag{28}$$

in which $\frac{\partial f(\boldsymbol{v}_u)}{\partial x_u}$ and $\frac{\partial f(\boldsymbol{v}_u)}{\partial y_u}$ are given in (29) and (30) (see bottom of the next page) and

$$\varphi_1(u,\chi_1,l,\chi_2,i) = \psi(u,\chi_1,l,\chi_2,i) g_1(\theta_{u,l}^{\chi_1}, \phi_{u,l}^{\chi_1}, \theta_{u,i}^{\chi_2}, \phi_{u,i}^{\chi_2}),$$
$$\varphi_2(u,\chi_1,l,\chi_2,i) = \psi(u,\chi_1,l,\chi_2,i) g_2(\theta_{u,l}^{\chi_1}, \theta_{u,i}^{\chi_2}). \quad (31)$$

Since $\|\nabla^2 f(\boldsymbol{v}_u)\|_2^2 \leq \|\nabla^2 f(\boldsymbol{v}_u)\|_F^2 = (\frac{\partial^2 f}{\partial {x_u}^2})^2 + (\frac{\partial^2 f}{\partial x_u \partial y_u})^2 + (\frac{\partial^2 f}{\partial {y_u}^2})^2 + (\frac{\partial^2 f}{\partial y_u \partial x_u})^2$, we can select δ_u as

$$\frac{8\pi^2}{\lambda^2}\left(\sum_{i=1}^{L_u^{\mathrm{r}}}\sum_{l=1}^{L_u^{\mathrm{r}}}|a_u^{i,l}| + \sum_{i=1}^{L_u^{\mathrm{r}}}\sum_{l=1}^{L_u^{\mathrm{d}}}|b_u^{i,l}| + \sum_{i=1}^{L_u^{\mathrm{d}}}\sum_{l=1}^{L_u^{\mathrm{r}}}|c_u^{i,l}| + \sum_{i=1}^{L_u^{\mathrm{d}}}\sum_{l=1}^{L_u^{\mathrm{d}}}|d_u^{i,l}|\right), \quad (35)$$

which satisfies $\delta_u \geq \|\nabla^2 f(\boldsymbol{v}_u)\|_F \geq \|\nabla^2 f(\boldsymbol{v}_u)\|_2$, and thus $\delta_u \boldsymbol{I}_2 \succeq \nabla^2 f(\boldsymbol{v}_u)$ based on eigenvalue decomposition. The second-order derivatives of f are given in (32), (33) and (34) (see bottom of this page), where

$$\Lambda_1(u,\chi_1,l,\chi_2,i) = \psi(u,\chi_1,l,\chi_2,i) g_1^2(\theta_{u,l}^{\chi_1}, \phi_{u,l}^{\chi_1}, \theta_{u,i}^{\chi_2}, \phi_{u,i}^{\chi_2}),$$
$$\Lambda_2(u,\chi_1,l,\chi_2,i) = \psi(u,\chi_1,l,\chi_2,i) g_2^2(\theta_{u,l}^{\chi_1}, \theta_{u,i}^{\chi_2}),$$
$$\Lambda_3(u,\chi_1,l,\chi_2,i) = \varphi_1(u,\chi_1,l,\chi_2,i) g_2(\theta_{u,l}^{\chi_1}, \theta_{u,i}^{\chi_2}). \quad (36)$$

Dropping the constraints of (26), (24) is transformed into

$$\max_{\boldsymbol{v}_u \in \mathcal{S}} -\frac{\delta_u}{2}\boldsymbol{v}_u^T \boldsymbol{v}_u + \left(\delta_u \boldsymbol{v}_u^{(i)} + \nabla f(\boldsymbol{v}_u^{(i)})\right)^T \boldsymbol{v}_u. \quad (37)$$

As the objective function of (37) is quadratic concave, it has the maximum value at $\boldsymbol{v}_u' = \boldsymbol{v}_u^{(i)} + \frac{\nabla f(\boldsymbol{v}_u^{(i)})}{\delta_u}$. If $\boldsymbol{v}_u'$ is inside $\mathcal{S}$, it is the solution of (37). Otherwise, we can obtain the solution using CVX. To obtain a good solution, we solve (24) using the SCA method from κ_{SCA} different initial points and let the position with the largest $f(\boldsymbol{v}_u)$ be the solution of problem (24). This method is summarized in Algorithm 1.

Since CVX utilizes an interior point method to solve a quadratic program, which usually results in high computational complexity, we propose the following gradient descent (GD) method with closed-form solution in each step.

3) GD based Method: Here, we adopt the GD method with backtracking line search to find the stationary points of $f(\boldsymbol{v}_u)$ [31, Chapter 9] . The antenna position of user u is updated by

$$\boldsymbol{v}_u^{(i+1)} = \boldsymbol{v}_u^{(i)} + \mu^{(i+1)} \nabla f(\boldsymbol{v}_u^{(i)}), \quad (38)$$

Algorithm 1 SCA for solving (24)

```
Let f* = 0.
for k=1:κ_SCA do
    Let i = 0.
    Initialize v_u^(i) which satisfies v_u ∈ S.
    repeat
        Calculate ∇f(v_u^(i)) and δ_u based on (28) and (35), respectively.
        Update v_u' = v_u^(i) + ∇f(v_u^(i)) / δ_u.
        if v_u' ∈ S then
            Update v_u^(i+1) = v_u'.
        else
            Obtain v_u, the solution of (37), using CVX.
            Update v_u^(i+1) = v_u.
        end if
        Let i = i + 1.
    until convergence
    if f(v_u^(i)) > f* then
        f* = f(v_u^(i)) and v_u* = v_u^(i).
    end if
end for
return v_u* as the solution of (24)
```

where $\mu^{(i+1)}$ is the step size for GD in the $(i+1)$-th iteration and $\nabla f(\boldsymbol{v}_u^{(i)})$ is the gradient in (28). Using the backtracking line search method, the step size μ starts at 1 and decreases by the factor $\beta \in (0,1)$ until the position is within the given antenna space and the Armijo-Goldstein condition is met, i.e.,

$$f(\boldsymbol{v}_u^{(i+1)}) \geqslant f(\boldsymbol{v}_u^{(i)}) + \alpha \mu^{(i+1)} \|\nabla f(\boldsymbol{v}_u^{(i)})\|_2^2, \quad (39)$$

where $\alpha \in (0, 0.5)$ is the control parameter for the step size.

Similar to the Section III-A2, we start the GD method from κ_{GD} random positions and select the result with the largest $f(\boldsymbol{v}_u)$ as the solution of (24). The main steps of the proposed gradient descent method are summarized in Algorithm 2.

$$\frac{\partial f(\boldsymbol{v}_u)}{\partial x_u} = j\frac{2\pi}{\lambda}\Big[\sum_{i=1}^{L_u^{\mathrm{r}}}\sum_{l=1}^{L_u^{\mathrm{r}}} a_u^{i,l}\varphi_1(u,\mathrm{r},l,\mathrm{r},i) + \sum_{i=1}^{L_u^{\mathrm{r}}}\sum_{l=1}^{L_u^{\mathrm{d}}} b_u^{i,l}\varphi_1(u,\mathrm{d},l,\mathrm{r},i) + \sum_{i=1}^{L_u^{\mathrm{d}}}\sum_{l=1}^{L_u^{\mathrm{r}}} c_u^{i,l}\varphi_1(u,\mathrm{r},l,\mathrm{d},i) + \sum_{i=1}^{L_u^{\mathrm{d}}}\sum_{l=1}^{L_u^{\mathrm{d}}} d_u^{i,l}\varphi_1(u,\mathrm{d},l,\mathrm{d},i)\Big], \quad (29)$$

$$\frac{\partial f(\boldsymbol{v}_u)}{\partial y_u} = j\frac{2\pi}{\lambda}\Big[\sum_{i=1}^{L_u^{\mathrm{r}}}\sum_{l=1}^{L_u^{\mathrm{r}}} a_u^{i,l}\varphi_2(u,\mathrm{r},l,\mathrm{r},i) + \sum_{i=1}^{L_u^{\mathrm{r}}}\sum_{l=1}^{L_u^{\mathrm{d}}} b_u^{i,l}\varphi_2(u,\mathrm{d},l,\mathrm{r},i) + \sum_{i=1}^{L_u^{\mathrm{d}}}\sum_{l=1}^{L_u^{\mathrm{r}}} c_u^{i,l}\varphi_2(u,\mathrm{r},l,\mathrm{d},i) + \sum_{i=1}^{L_u^{\mathrm{d}}}\sum_{l=1}^{L_u^{\mathrm{d}}} d_u^{i,l}\varphi_2(u,\mathrm{d},l,\mathrm{d},i)\Big], \quad (30)$$

$$\frac{\partial^2 f}{\partial {x_u}^2} = \frac{-4\pi^2}{\lambda^2}\Big[\sum_{i=1}^{L_u^{\mathrm{r}}}\sum_{l=1}^{L_u^{\mathrm{r}}} a_u^{i,l}\Lambda_1(u,\mathrm{r},l,\mathrm{r},i) + \sum_{i=1}^{L_u^{\mathrm{r}}}\sum_{l=1}^{L_u^{\mathrm{d}}} b_u^{i,l}\Lambda_1(u,\mathrm{d},l,\mathrm{r},i) + \sum_{i=1}^{L_u^{\mathrm{d}}}\sum_{l=1}^{L_u^{\mathrm{r}}} c_u^{i,l}\Lambda_1(u,\mathrm{r},l,\mathrm{d},i) + \sum_{i=1}^{L_u^{\mathrm{d}}}\sum_{l=1}^{L_u^{\mathrm{d}}} d_u^{i,l}\Lambda_1(u,\mathrm{d},l,\mathrm{d},i)\Big], \quad (32)$$

$$\frac{\partial^2 f}{\partial {y_u}^2} = \frac{-4\pi^2}{\lambda^2}\Big[\sum_{i=1}^{L_u^{\mathrm{r}}}\sum_{l=1}^{L_u^{\mathrm{r}}} a_u^{i,l}\Lambda_2(u,\mathrm{r},l,\mathrm{r},i) + \sum_{i=1}^{L_u^{\mathrm{r}}}\sum_{l=1}^{L_u^{\mathrm{d}}} b_u^{i,l}\Lambda_2(u,\mathrm{d},l,\mathrm{r},i) + \sum_{i=1}^{L_u^{\mathrm{d}}}\sum_{l=1}^{L_u^{\mathrm{r}}} c_u^{i,l}\Lambda_2(u,\mathrm{r},l,\mathrm{d},i) + \sum_{i=1}^{L_u^{\mathrm{d}}}\sum_{l=1}^{L_u^{\mathrm{d}}} d_u^{i,l}\Lambda_2(u,\mathrm{d},l,\mathrm{d},i)\Big], \quad (33)$$

$$\frac{\partial^2 f}{\partial x_u \partial y_u} = \frac{\partial^2 f}{\partial y_u \partial x_u} = \frac{-4\pi^2}{\lambda^2}\Big[\sum_{i=1}^{L_u^{\mathrm{r}}}\sum_{l=1}^{L_u^{\mathrm{r}}} a_u^{i,l}\Lambda_3(u,\mathrm{r},l,\mathrm{r},i) + \sum_{i=1}^{L_u^{\mathrm{r}}}\sum_{l=1}^{L_u^{\mathrm{d}}} b_u^{i,l}\Lambda_3(u,\mathrm{d},l,\mathrm{r},i) + \sum_{i=1}^{L_u^{\mathrm{d}}}\sum_{l=1}^{L_u^{\mathrm{r}}} c_u^{i,l}\Lambda_3(u,\mathrm{r},l,\mathrm{d},i) + \sum_{i=1}^{L_u^{\mathrm{d}}}\sum_{l=1}^{L_u^{\mathrm{d}}} d_u^{i,l}\Lambda_3(u,\mathrm{d},l,\mathrm{d},i)\Big], \quad (34)$$

Algorithm 2 GD for solving (24)

Let $f^* = 0$.
for k=1:κ_{GD} **do**
  Initialize $\boldsymbol{v}_u^{(1)}$ which satisfies $\boldsymbol{v}_u \in \mathcal{S}$. Let $i = 0$.
  repeat
    Let $i = i + 1$.
    Calculate $f(\boldsymbol{v}_u^{(i)})$ and $\nabla f(\boldsymbol{v}_u^{(i)})$ based on (23) and (28), respectively.
    Initialize $\mu^{(i+1)} = 1$.
    repeat
      Let $\mu^{(i+1)} = \beta\mu^{(i+1)}$.
      Update $\boldsymbol{v}_u^{(i+1)} = \boldsymbol{v}_u^{(i)} + \mu^{(i+1)}\nabla f(\boldsymbol{v}_u^{(i)})$.
      Calculate $f(\boldsymbol{v}_u^{(i+1)})$.
    until Armijo-Goldstein condition in (39) is satisfied.
  until convergence
  if $f(\boldsymbol{v}_u^{(i+1)}) > f^*$ **then**
    $f^* = f(\boldsymbol{v}_u^{(i+1)})$ and $\boldsymbol{v}_u^* = \boldsymbol{v}_u^{(i+1)}$.
  end if
end for
return $\boldsymbol{v}_u^*$ as the solution of (24)

B. Complexity Analysis

For convenience, it is assumed that the number of propagation paths for each channel is identical, i.e., $L_u^{\text{d}} = L_{\text{br}} = L_u^{\text{r}} = L, \forall u \in \mathcal{U}$. Noting that the complexity of calculating $\boldsymbol{A}_u$, $\boldsymbol{B}_u$, $\boldsymbol{C}_u$, and $\boldsymbol{D}_u$ is $F = NML + M^2U + M^2L$, the complexity of ES is then $\mathcal{O}((K+1)^2L^2 + F)$. Denoting the maximum number of iterations by N_{SCA}, the complexity of Algorithm 1 is $\mathcal{O}(\kappa_{\text{SCA}}N_{\text{SCA}}L^2 + F)$. The implementation of Algorithm 2 has a complexity of $\mathcal{O}(\kappa_{GD}N_{\text{out}}(N_{\text{in}}L^2+L^2)+F)$, where N_{in} and N_{out} are the maximum number of iterations of the inner and outer loops of Algorithm 2, respectively. The complexity of solving (19) is $\mathcal{O}(UO_s)$, where O_s is the complexity of the chosen method among ES, SCA, and GD.

IV. Simultion Results

In this section, we verify the performance of the proposed algorithms through Monte Carlo simulations. The carrier frequency is 30 GHz. The noise power σ_u^2 is set to be -80 dBm. The azimuth and elevation of AoAs and AoDs follow uniform distribution over $[0, \pi]$. For convenience, we assume the same number of propagation paths for each channel and the same SINR target for each user, i.e., $L_u^{\text{d}} = L_u^{\text{r}} = L_{\text{br}} = L$, $\epsilon_u = \epsilon$, $\forall u \in \mathcal{U}$. In addition, we set $\alpha = 0.1$, $\beta = 10^{-3}$, $K = 5$, $\kappa_{\text{SCA}} = 100$, $\kappa_{\text{GD}} = 10$, and $d_{\text{BS}} = d_{\text{r}} = \lambda/2$. The performance of the strategy that uses FPAs at the users is given as a benchmark for transmit power comparison.

In Fig. 2, we study how the transmit power changes with a user antenna position when the other user antennas are located at the origin $(0, 0)$. We can observe that the required power at different locations varies from -10 dB to 0 dB, which shows the necessity of starting SCA and GD schemes from different initial points to avoid getting stuck in local maxima.

Now, Fig. 3 depicts the minimum transmit power over the number of users U under different SINR targets ϵ. Since each user is equipped with a single fluid antenna, increasing the number of users also introduces more degrees of freedom into the system. Therefore, the power savings achieved with fluid antennas compared to FPAs grow as U increases. Specifically, as U increases from 2 to 6, the power saved by fluid antennas increases from 1 dB (26%) to 2 dB (58%) for both SINR targets ($\epsilon = 3$ dB and $\epsilon = 5$ dB).

Finally, Fig. 4 investigates the effect of FAS size on the transmit power. Since a large antenna provides more spatial diversity, the transmit power of using GD or SCA initially decreases with the normalized antenna size. Due to the fact that the antenna with large space can cover enough local optimal points, further increasing the antenna size does not bring any more power reduction. As a result, the transmit power reaches saturation when the antenna size is about 5λ. In contrast, the transmit power for the ES scheme increases slightly with antenna size. This is because we maintain a fixed number of search points on each fluid antenna, which leads to a decrease

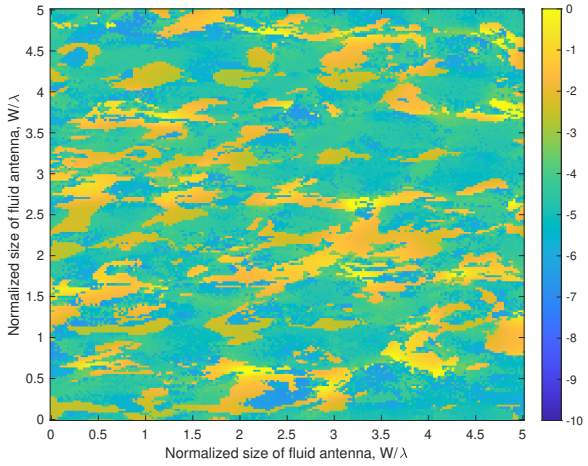

Fig. 2. Transmit power versus the antenna locations with $\epsilon = 3$ dB, $N_1 = N_2 = 5$, $M = 5$, $L = 10$ and $U = 5$.

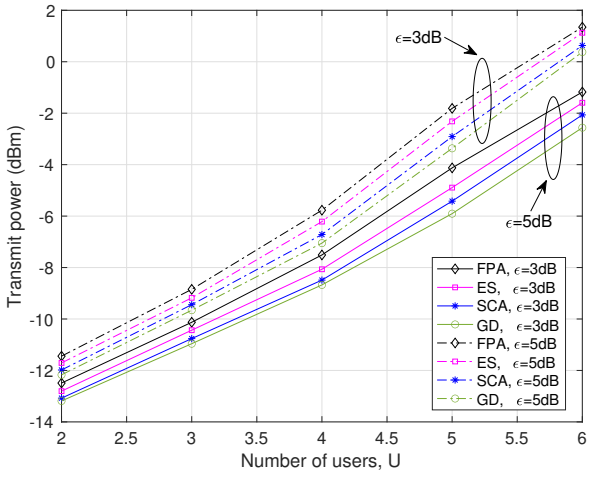

Fig. 3. Transmit power versus the number of users with $W = 3\lambda$, $M = 6$, $N_1 = N_2 = 5$, and $L = 10$.

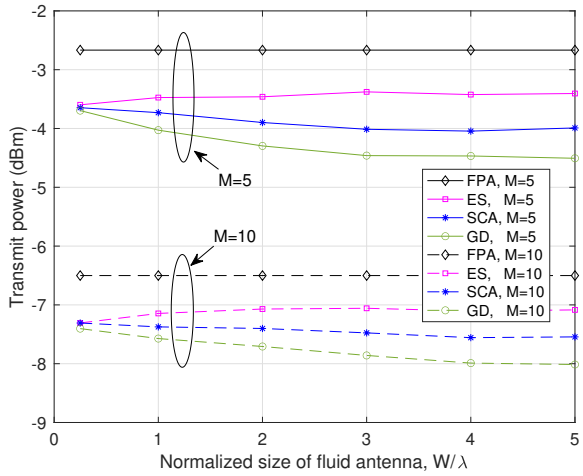

Fig. 4. Transmit power versus normalized size of fluid antenna with $\epsilon = 3$ dB, $L = 10$, $N_1 = N_2 = 5$ and $U = 5$.

in search resolution as the antenna size increases.

V. Conclusion

In this letter, we studied the power minimization problem of a FAS-RIS-aided downlink system under QoS constraints. We have addressed the problem by iteratively optimizing the precoding vectors, the phase shift of RIS, and the FAS antenna positions. ES, SCA, and GD methods were developed to find the optimal antenna position of each user, while the precoding vectors and phase shift of RIS were optimized by a classical algorithm. Simulation results showed that FAS requires much less transmit power to achieve the target SINR than FPA. This work assumed perfect CSI, which is difficult to obtain in real-world applications and that CSI errors may cause the actual SINR to fall below the threshold, making the optimization problem infeasible. In the future, robust optimization algorithms should be sought to account for the imperfect CSI case. In addition, the physical power consumption and reconfiguration time of the RIS and FAS may affect system performance. Future work is suggested to consider hardware limitations to offer valuable insights for real-world applications.

References

[1] K. K. Wong, A. Shojaeifard, K.-F. Tong, and Y. Zhang, "Fluid antenna systems," *IEEE Trans. Wireless Commun.*, vol. 20, no. 3, pp. 1950–1962, Mar. 2021.

[2] W. K. New *et al.*, "A tutorial on fluid antenna system for 6G networks: Encompassing communication theory, optimization methods and hardware designs," *IEEE Commun. Surv. & Tuts.*, doi:10.1109/COMST.2024.3498855, 2024.

[3] B. Tang *et al.*, "Fluid antenna enabling secret communications," *IEEE Commun. Lett.*, vol. 27, no. 6, pp. 1491–1495, Jun. 2023.

[4] K. K. Wong and K.-F. Tong, "Fluid antenna multiple access," *IEEE Trans. Wireless Commun.*, vol. 21, no. 7, pp. 4801–4815, Jul. 2022.

[5] H. Xu *et al.*, "Capacity maximization for FAS-assisted multiple access channels," *IEEE Trans. Commun.*, doi:10.1109/TCOMM.2024.3516499, 2024.

[6] Y. Shen *et al.*, "Design and implementation of mmWave surface wave enabled fluid antennas and experimental results for fluid antenna multiple access," *arXiv preprint*, arXiv:2405.09663, May 2024.

[7] J. Zhang *et al.*, "A novel pixel-based reconfigurable antenna applied in fluid antenna systems with high switching speed," *IEEE Open J. Antennas Propag.*, vol. 6, no. 1, pp. 212–228, Feb. 2025.

[8] B. Liu, K. F. Tong, K. K. Wong, C.-B. Chae, and H. Wong, "Be water, my antennas: Riding on radio wave fluctuation in nature for spatial multiplexing using programmable meta-fluid antenna," *arXiv preprint*, arXiv:2502.04693, 2025.

[9] L. Zhu and K. K. Wong, "Historical review of fluid antenna and movable antenna," *arXiv preprint*, arXiv:2401.02362v2, 2024.

[10] H. Xu *et al.*, "Revisiting outage probability analysis for two-user fluid antenna multiple access system," *IEEE Trans. Wireless Commun.*, vol. 23, no. 8, pp. 9534–9548, Aug. 2024.

[11] Y. Chen, S. Li, Y. Hou, and X. Tao, "Energy-efficiency optimization for slow fluid antenna multiple access using mean-field game," *IEEE Wireless Commun. Lett.*, vol. 13, no. 4, pp. 915–918, Apr. 2024.

[12] J. Yao *et al.*, "Exploring fairness for FAS-assisted communication systems: From NOMA to OMA," *IEEE Trans. Wireless Commun.*, vol. 24, no. 4, pp. 3433–3449, Apr. 2025

[13] C. Wang *et al.*, "Fluid antenna system liberating multiuser MIMO for ISAC via deep reinforcement learning," *IEEE Trans. Wireless Commun.*, vol. 23, no. 9, pp. 10879–10894, Sept. 2024.

[14] Q. Zhang, M. Shao, T. Zhang, G. Chen, and J. Liu, "An efficient algorithm for sum-rate maximization in fluid antenna-assisted ISAC system," *arXiv preprint*, arXiv:2405.06516, May 2024.

[15] Y. Zuo *et al.*, "Fluid antenna for mobile edge computing," *IEEE Commun. Lett.*, vol. 28, no. 7, pp. 1728–1732, Jul. 2024.

[16] N. Waqar *et al.*, "Opportunistic fluid antenna multiple access via team-inspired reinforcement learning," *IEEE Trans. Wireless Commun.*, vol. 23, no. 9, pp. 12068–12083, Sept. 2024.

[17] R. Xu *et al.*, "Fluid antenna relay assisted communication systems through antenna location optimization," in *Proc. IEEE Int. Conf. Commun. (ICC) Workshops*, Denver, CO, USA, pp. 1140–1145, Jun. 2024.

[18] L. Zhang, H. Yang, Y. Zhao, and J. Hu, "Joint port selection and beamforming design for fluid antenna assisted integrated data and energy transfer," *IEEE Wireless Commun. Lett.*, vol. 13, no. 7, pp. 1833–1837, Jul. 2024.

[19] Q. Wu and R. Zhang, "Intelligent reflecting surface enhanced wireless network via joint active and passive beamforming," *IEEE Trans. Wireless Commun.*, vol. 18, no. 11, pp. 5394–5409, Nov. 2019.

[20] K. Meng, Q. Wu, W. Chen and D. Li, "Sensing-assisted communication in vehicular networks with intelligent surface," *IEEE Trans. Veh. Technol.*, vol. 73, no. 1, pp. 876–893, Jan. 2024

[21] F. R. Ghadi *et al.*, "On performance of RIS-aided fluid antenna systems," *IEEE Wireless Commun. Lett.*, vol. 13, no. 8, pp. 2175–2179, Aug. 2024.

[22] L.-H. Shen and Y.-H. Chiu, "RIS-aided fluid antenna array-mounted AAV networks," *IEEE Wireless Commun. Lett.*, vol. 14, no. 4, pp. 1049–1053, Apr. 2025.

[23] Y. Sun *et al.*, "Sum-rate optimization for RIS-aided multiuser communications with movable antennas," *IEEE Wireless Commun. Lett.*, vol. 14, no. 2, pp. 450–454, Feb. 2025.

[24] J. Zhu *et al.*, "Fluid antenna empowered index modulation for RIS-aided mmWave transmissions," *IEEE Trans. Wireless Commun.*, vol. 24, no. 2, pp. 1635–1647, Feb. 2025.

[25] J. Ye, P. Zhang, X.-P. Li, L. Huang, and Y. Liu, "Joint beamforming and position optimization for fluid RIS-aided ISAC systems," *arXiv preprint*, arXiv:2501.13339, Jan. 2025.

[26] A. Salem, K.-K. Wong, G. Alexandropoulos, C.-B. Chae, and R. Murch, "A first look at the performance enhancement potential of fluid reconfigurable intelligent surface," *arXiv preprint*, arXiv:2502.17116, 2025.

[27] H. Xu *et al.*, "Channel estimation for FAS-assisted multiuser mmWave systems," *IEEE Commun. Lett.*, vol. 23, no. 3, pp. 632–636, Mar. 2024.

[28] W. Mei, X. Wei, B. Ning, Z. Chen and R. Zhang, "Movable-antenna position optimization: A graph-based approach," *IEEE Wireless Commun. Lett.*, vol. 13, no. 7, pp. 1853–1857, Jul. 2024.

[29] Y. Wu, D. Xu, D. W. K. Ng, W. Gerstacker and R. Schober, "Movable antenna-enhanced multiuser communication: Jointly optimal discrete antenna positioning and beamforming," in *Proc. IEEE Global Commun. Conf. (GLOBECOM)*, pp. 7508–7513, Dec. 2023, Kuala Lumpur, Malaysia.

[30] M. Hong, Q. Li, and Y.-F. Liu, "Decomposition by successive convex approximation: A unifying approach for linear transceiver design in heterogeneous networks," *IEEE Trans. Wireless Commun.*, vol. 15, no. 2, pp. 1377–1392, Feb. 2016.

[31] S. P. Boyd and L. Vandenberghe, *Convex Optimization*. Cambridge university press, 2004.